AO12: Rapid detection of volcanic ash with the Cross-track Infrared Sounder

Candidate number: 1063879
Supervisors: I.A. Taylor and R.G. Grainger

Abstract

An atmospheric trace species retrieval algorithm developed by Walker et al [1] has been adapted to detect volcanic ash using data from the Cross-track Infrared Sounder (CrIS). Results for the April 2021 eruption of La Soufrière St. Vincent are compared with a similar ash retrieval developed for the Infrared Atmospheric Sounding Interferometer (IASI). There is good agreement between the results—doubling the temporal resolution of volcanic ash detection compared with using the IASI instrument alone. La Soufrière results are also shown to agree well with official ash guidance generated by the Washington Volcanic Ash Advisory Centre (VAAC). The retrieval was also run on the January 2022 eruption of Hunga Tonga-Hunga Ha'apai (HT-HH) and the results were shown to correlate well with the known timeline of the eruption and produce a convincing ash cloud trajectory.

1 Introduction

1.1 Motivation

Airborne volcanic ash is a major hazard of volcanic eruptions [2]. Volcanic ash is particularly dangerous to aircraft as it reduces visibility and can cause engine failure [2]. Following significant ash cloud encounters, where passenger planes were severely damaged in 1982 and 1990, nine regional meteorological agencies were designated as VAACs [3]. They were tasked with providing global tracking of volcanic ash clouds and producing the relevant aviation guidance [3]. A lack of knowledge of safe ash levels for aviation meant the initial guidance was to avoid all ash [3]. This was successful until the Eyjafjallajökull eruption of 2010 when 95,000 flights were disrupted [3] which led to the rules being relaxed and three zones of ash concentration being introduced in Europe [4]. The lowest concentration zone, which aircraft are now permitted to fly through, has a minimum ash concentration of 200 $\mu g\,m^{-3}$, which was the previous concentration for no-fly guidance [4]. The other two zones are set at levels of 2,000 and 4,000 $\mu g\,m^{-3}$ and these can only be flown through with special permission. Benefits of these rule changes were seen the next year when an even larger eruption in Iceland, Grímsvötn, only cancelled 900 flights [4]. The introduction of ash mass concentration limits has posed significant challenges to the ash tracking community, as current methods for quantifying ash concentrations have coarser resolutions than the concentration thresholds [4]. Indeed, the ash retrieval presented in this paper remains entirely qualitative.

Satellite data is a particularly important part of volcanic ash surveillance as it allows monitoring of volcanos in underfunded and remote places [5]. It is the primary source VAACs use to produce advice [6] alongside ground observations, radiosondes and dispersion models [7]. However, satellite observation of ash by infrared techniques, such as those used in this paper, struggle to differentiate volcanic and meteorological clouds, leading to potential delays in identification of eruptions [6]. Given the risks to aviation from ash, and the economic benefits of more nuanced advisories derived from ash concentration estimates, better satellite volcanic ash surveillance will both increase safety and decrease cancellations of flights.

1.2 The Instruments: CrIS and IASI

In this paper a volcanic ash retrieval algorithm (discussed in Section 2), originally developed for use with the IASI instrument's data, was adapted to use data from the CrIS instrument.

CrIS is an interferometer flying on three polar-orbiting satellites—the Suomi National Polar-orbiting Partnership (SNPP), launched in Jan-

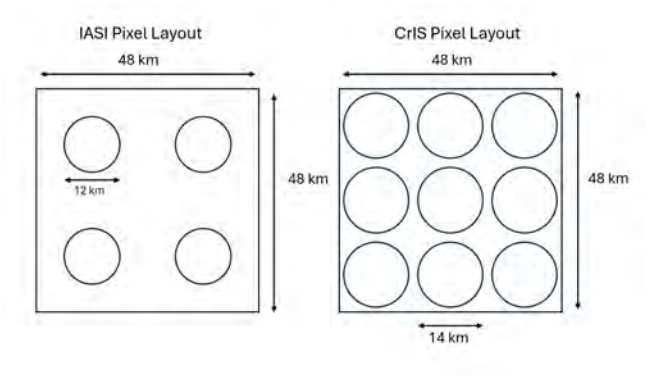

Figure 1: Different pixel layouts for CrIS and IASI. Each circle is an observation pixel.

uary 2012; the Joint Polar Satellite System-1 (JPSS-1), launched in February 2018; and the Joint Polar Satellite System-2, launched in November 2023. A further two instruments are planned to be launched in 2027 and 2033 [8]. The currently active satellites are in sun-synchronous orbits which have equatorial crossing times (EQTs) of 13:25 Local Time (LT) on their ascent [8]. For the eruption of La Soufrière data from only two satellites, JPSS-1 and SNPP, were processed. For the eruption of HT-HH, only data from JPSS-1 was processed. CrIS measures radiation in three separate infrared bands: 650 – 1095, 1210 – 1750, and 2155 – 2550 cm^{-1}, which have resolutions of 0.625, 1.25, and 2.5 cm^{-1}, respectively. This paper uses the first range of wavenumbers since this region has sensitivity to ash [9].

IASI is an interferometer similar to CrIS. It measures radiation in the bands 645 – 1210, 1210 – 2000, and 2000 – 2760 cm^{-1}, all with resolutions of 0.25 cm^{-1}. This paper compares ash retrievals using IASI and CrIS data for the eruption of La Soufrière in April 2021. During this eruption, IASI was aboard 3 satellites in sun-synchronous orbits, two of which had EQTs at 09:31 LT and the other at 07:31 LT on their descents [8]. A key difference between these instruments is their spatial resolution. Both instruments observe the Earth in steps of 48 x 48 km cells at nadir but CrIS captures nine 14 km diameter circular pixels per cell whereas IASI only captures four 12 km diameter circular pixels per cell as shown in Figure 1.

Table 1 summarises the spectral ranges and resolutions, as well as the temperature sensitivities (minimum measurable temperature differences) of the instruments.

Table 1: Spectral and temperature resolutions for CrIS and IASI across their respective wavelength bands. Data from [8].

Instrument	Spectral Band (cm^{-1})	Resolution (cm^{-1})	Temperature Sensitivity (K) (@ Scene Temp)
CrIS	650 – 1095	0.625	0.24 – 0.39 @ 287 K
	1210 – 1750	1.25	0.19 – 0.28 @ 287 K
	2155 – 2550	2.5	0.18 – 0.21 @ 287 K
IASI	645 – 1200	0.25	0.2 – 0.3 @ 280 K
	1200 – 2000	0.25	0.2 – 0.5 @ 280 K
	2000 – 2760	0.25	0.5 – 2 @ 280 K

1.3 Previous Work

Walker et al [1] used an optimally weighted one-step retrieval algorithm to detect volcanic SO_2 and agricultural NH_3 using the IASI instrument. This makes full use of the spectral range of the instrument compared with previous brightness temperature difference methods which only utilise a few spectral channels. This results in retrievals with sensitivity improved by up to an order of magnitude, without compromising on computation speed. In this paper, Walker's method is adapted to detect volcanic ash with CrIS.

2 Methods

The ash detection method of this report comes from Walker et al [1] who describes it as "essentially an optimally weighted one-step retrieval" and is as follows:

First, spectral measurements are assumed to take the form:

$$\vec{y} = F(\vec{x}, \vec{u}) + \epsilon_{rnd} + \epsilon_{sys} \tag{1}$$

where, $\vec{x} = [x_c, \text{ off}]^T$ is the "true state vector", x_c is the target species column amount, off is some wavelength-independent brightness temperature offset, $\vec{u}$ is the best estimate of other relevant parameters (instrument, atmosphere, and surface properties), ϵ_{rnd} is random measurement error, ϵ_{sys} is the systematic error and F is the forward model.

If F is nearly linear about climatological conditions, Equation (1) can be approximated as:

$$\vec{y} - F(\vec{x_0}, \vec{u}) = \vec{K}(\vec{x} - \vec{x_0}) + \epsilon_{rnd} + \epsilon_{sys} \tag{2}$$

where $\vec{x_0} = [x_{c0}, 0]^T$ is the linearisation point (x_{c0} is the climatological column amount of the target species) and $\vec{K}$ is the Jacobian, which gives the rate of change of the measured spectra per unit of the target species column amount. The Jacobian is discussed further in Section 2.1.

The next step is to minimise the difference between the modelled and observed spectra while weighting with the inverse covariance matrix so that the channels in the spectra with the highest errors contribute the least to the retrieval [10]. Minimise:

$$||\Delta\vec{y} - \vec{K}(\vec{x} - \vec{x_0})||^2_{S_{tot}^{-1}} \quad (3)$$

here $||\vec{v}||^2_{S_{tot}^{-1}}$ denotes $\vec{v}^T S_{tot}^{-1}\vec{v}$ and $\Delta\vec{y}$ is $\vec{y} - \langle\vec{y}\rangle$ with $\langle\vec{y}\rangle$ being the mean spectrum in climatological conditions. S_{tot} is a covariance matrix generated from spectra collected one year prior to the eruption of interest in the same geographical location and month of the eruption. The covariance matrix is how the random and systematic errors of the different channels in the spectra are quantified and represents the spectral variability of the climatological background. See Section 2.2 for more details. Differentiating Equation (3) with respect to $\Delta x = \vec{x} - \vec{x_0}$, setting to zero, and rearranging gives

$$\vec{x} = \vec{x_0} + (\vec{K}^T S_{tot}^{-1}\vec{K})^{-1}\vec{K}^T S_{tot}^{-1}\Delta\vec{y} \quad (4)$$

$(\vec{K}^T S_{tot}^{-1}\vec{K})$ is called the "measurement contribution function". The first row of which is denoted $\vec{g_c}^T$. From this, the column amount of the target species can be extracted:

$$x_c = \vec{g_c}^T(\vec{y} - \langle\vec{y}\rangle) \quad (5)$$

The retrieved column amount, x_c, is in units of ash optical depth (AOD) at 10 µm but is not an accurate measure of that quantity due to various limitations (see Section 2.3). It can only be used as an indicator for whether ash levels are enhanced compared to the background.

2.1 The Jacobian

The Jacobians, $\vec{K}$, used in the retrieval calculations were calculated using the Reference Forward Model (RFM), which is a line-by-line radiative transfer model [11]. It takes as inputs the properties of the atmosphere and outputs the expected top of atmosphere brightness temperature spectra i.e. the spectra that an interferometer aboard a satellite should observe. Spectra were generated with and without the presence of a 2 km thick layer of ash in the atmosphere and the difference between these was used as the Jacobian. The units of the Jacobian are K τ^{-1} where τ is an optical depth for a specific wavelength and K is kelvin. Conveniently, the ash file used resulted in an optical depth of 1 at 10 µm and so the 'column amount' retrieved in Equation (5) is in units of optical depth at 10 µm. The ash extinction profile fed into the RFM was generated with ash properties (refractive index and size distribution) from an eruption of Mt. Aso in Japan.

The way the Jacobians were generated gives the retrieval some limitations and contribute to the qualitative nature of the method. Namely, the ash extinction profile inputted into the RFM was arbitrary and not necessarily related to the type of ash erupting from a specific volcano. In addition to the extinction profile, the RFM also needs to know the height and thickness of the ash layer. Unless otherwise stated, the retrievals in this paper assume a 2 km thick layer of ash at an altitude of 20 km. This was chosen to represent stratospheric eruptions, but is not applicable to all eruptions. Different heights of ash layers are investigated in Section 3.

2.2 The Covariance Matrix

The covariance matrix is used in the retrieval to represent the background variability in the observed spectra. A large region was chosen around the area the ash cloud was known to span and the observed spectra were analysed to calculate the covariance matrix as follows [12]: given a large array of N spectra,

$$\vec{Y} = [\vec{y_1}\ \vec{y_2}\ ...\ \vec{y_N}] \quad (6)$$

where each $\vec{y_i}$ is the spectra at a pixel and has the same number of elements as the number of channels. The mean vector is defined as

$$\langle\vec{y}\rangle = \frac{1}{N}\sum_{i=1}^{N}\vec{y_i} \quad (7)$$

Smith [12] then shows that the covariance matrix can be calculated as

$$\vec{S} = \frac{1}{N-1}(\vec{Y}\vec{Y}^T - N\langle\vec{y}\rangle\langle\vec{y}\rangle^T) \quad (8)$$

This is computationally slow [12] and so the data is split such that $\vec{Y} = [\vec{Y_1}\ \vec{Y_2}]$, $\langle\vec{y}\rangle = \frac{N_1\langle\vec{y}\rangle_1 + N_2\langle\vec{y}\rangle_2}{N_1+N_2}$, and $\vec{Y}\vec{Y}^T = \vec{Y_1}\vec{Y_1}^T + \vec{Y_2}\vec{Y_2}^T$, the total covariance matrix can then be calculated as

$$S_{tot} = \frac{1}{N-1}\sum_{i=1}^{L}\vec{Y_i}\vec{Y_i}^T - N\langle\vec{y}\rangle\langle\vec{y}\rangle^T \quad (9)$$

where L is the number of subsets the data is split into.

Separate covariance matrices were generated for the different CrIS instruments to account for differences in their observed spectra. Different covariance matrices were also generated separately for each eruption studied in this paper. As this was a preliminary study, eruptions producing volcanic clouds over ocean were chosen. This makes the retrieval simpler as Tichford [13] found that covariance matrices generated over land had significantly larger values than those generated over ocean. This means that to accurately represent the background in the retrieval, separate covariance matrices would need to be generated over land and possibly even over different biomes [13]. Tichford [13] also found the presence of meteorological clouds to have a large impact on the resulting covariance matrix. Future work could involve producing dedicated retrievals for cloud-covered pixels by using covariance matrices and mean spectra generated specifically from cloudy conditions. This was beyond the scope of this study, further contributing to the qualitative nature of the retrievals.

2.3 Limitations

Table 2 summarises some of the limitations discussed so far as well as others to be discussed later. These limitations result in the method being a qualitative ash detection technique that cannot retrieve ash mass concentrations, which—as mentioned in the introduction—are required to define no-fly zones. Calibrating the retrieved AOD to ash mass concentration, for example using radiosondes, would be a valuable next step for future work.

2.4 Detection Threshold

The method used in this paper is qualitative and uses a simple detection threshold to flag probable ash pixels. This involves flagging all pixels with an AOD greater than a certain Z-number of standard deviations above zero. The standard deviation, σ, following Rodgers [10] was calculated as:

$$\sigma = \left(\mathbf{K}^{\mathrm{T}}{\mathbf{S_{tot}}}^{-1}\mathbf{K}\right)^{-\frac{1}{2}}$$

The required Z-number was chosen by eye by plotting the retrievals with a range of Z-number thresholds and choosing one which flagged the likely ash cloud while keeping false positives low. For example, Figure 2 shows the different flagged pixel distributions for varying Z-numbers for the retrieval of the La Soufrière volcanic cloud for the CrIS instrument aboard SNPP. A Z-number of 10 was chosen for the SNPP CrIS instrument as a good compromise between false positives and negatives. The CrIS instrument on JPSS-1 showed much less noise and so a threshold Z-number of 7.5 was chosen. Pery [15] hypothesised that the reason for the CrIS on SNPP having significantly higher noise was due to it being in service for 6 more years then the one aboard JPSS-1. Also, it was found during validation that the CrIS on SNPP had a sensor with a significantly elevated noise level [16], which would likely increase the noise of the retrieval.

Current Limitation	Potential Solution/Improvements
Meteorological clouds affect retrieval AOD [13].	Use separate covariance matrices for cloudy and cloud-free areas.
Dust is flagged as ash as they are spectrally similar [14].	Generate separate covariance matrices and mean spectra for high dust concentration areas (e.g. deserts).
Jacobian based on an unrepresentative ash sample.	Generate Jacobians for various ash heights and types, run separate retrievals, then sum retrieval flags per pixel.
Different biomes are spectrally dissimilar [13].	Use separate covariance matrices and mean spectra for different biomes.

Table 2: Current limitations of the linear retrieval technique and potential solutions.

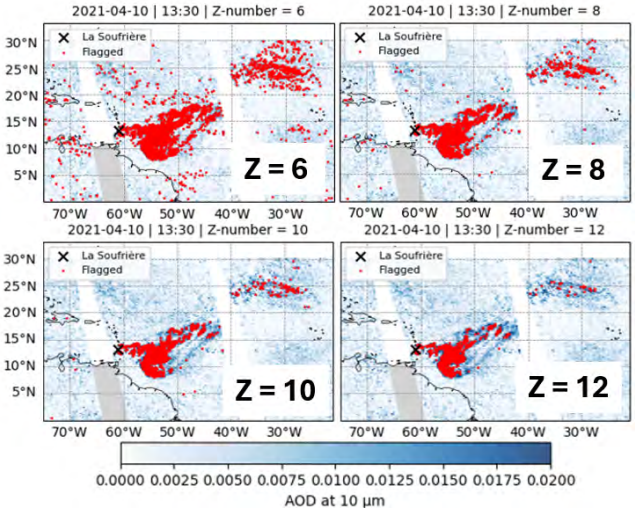

Figure 2: Ash flag distributions with varying threshold Z-numbers for SNPP CrIS ash retrieval of La Soufrière. All times in LT.

3 Results and Discussion

This paper analyses the eruptions of HT-HH in January 2022 and La Soufrière in April

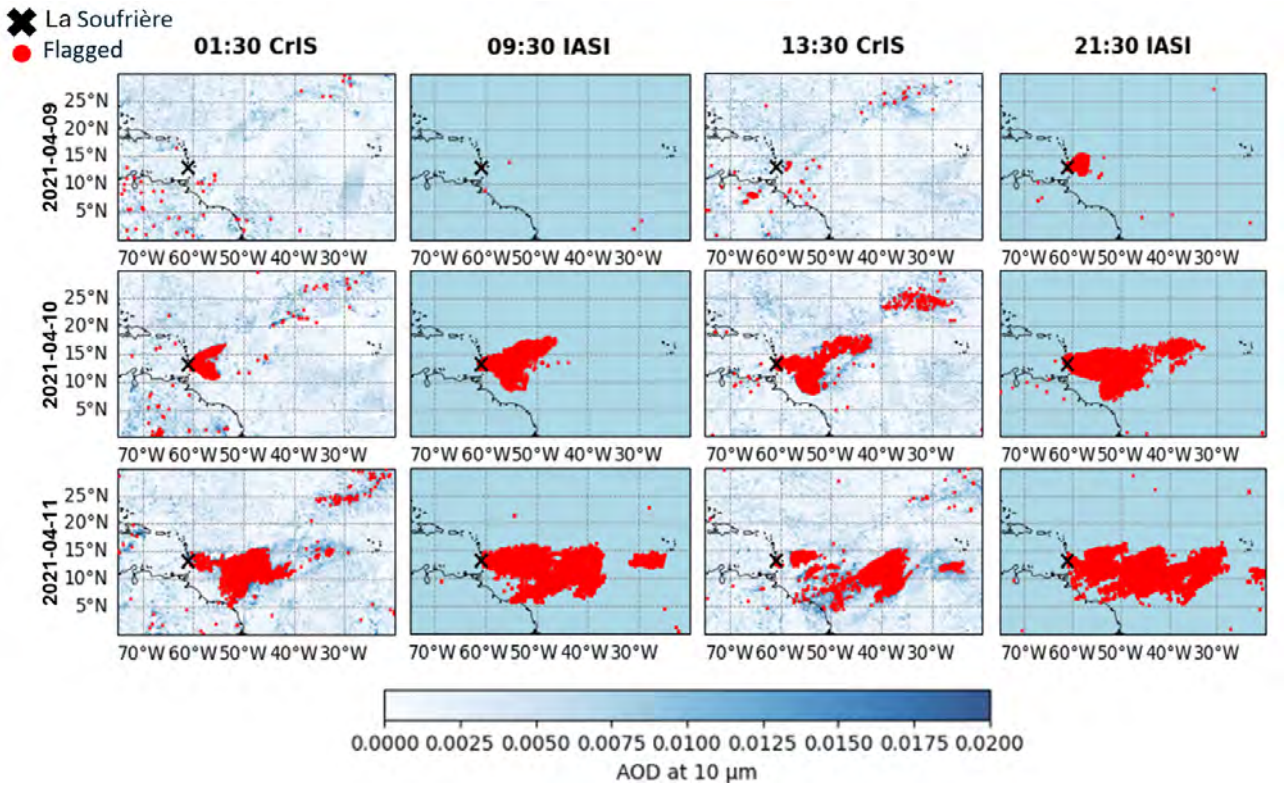

Figure 3: IASI and CrIS ash retrievals for the April 2021 eruption of La Soufrière arranged in chronological order. Colour bar only for use with the CrIS scenes. Times are local.

2021. These eruptions were chosen because the ash clouds largely travel above ocean, making the retrieval calculation simpler as discussed in Section 2.2. The retrieval for La Soufrière is compared with IASI ash retrievals generated in EODG and published by Taylor et al [17], official Washington VAAC ash advisories, and accounts of the eruption timeline. The HT-HH results are compared with the reported eruption timeline and red green blue (RGB) colour maps produced by Sellitto et al [18]. IASI results and VAAC ash advisories were not available for the HT-HH eruption.

3.1 La Soufrière

La Soufrière, located on the island of St. Vincent, is one of the most active volcanos in the eastern Caribbean [19]. It has erupted four times since 1902 [20] and previous eruptions have resulted in mass fatalities [19]. The eruption studied in this paper led to $\sim$ 16,000 evacuations, with displaced residents not beginning to return until the 15$^{\text{th}}$ of September despite the eruption officially ending on the 22$^{\text{nd}}$ of April due to continued risk of further activity [19].

Figure 3 shows the La Soufrière linear ash retrieval results generated in this paper (CrIS) placed side by side with IASI ash retrievals generated in the Earth Observation Data Group (EODG) by Taylor et al [17]. The times given as column headers are near to the local time that these observations occurred based on the EQTs of the relevant satellites. The eruption began at 08:40 LT on the 9$^{\text{th}}$ of April with an explosion generating an ash cloud which drifted ENE [20]. The CrIS results show some activity near the volcano for the first observation after this (13:30 LT on the 9$^{\text{th}}$) but this is difficult to discern from noise. IASI clearly picks out an ash cloud at its next observation (21:30 LT on the 9$^{\text{th}}$) and this cloud then grows and moves ENE in both the CrIS and IASI retrievals. This matches observations well with the Global Volcanism Program (GVP) [20] reporting multiple events feeding the cloud for hours on the 9$^{\text{th}}$ and eruptive activity continuing for the following 2 weeks. GVP [20] further reports that the cloud travelled around 1,200 km ESE and 3,000 km ENE by the end of the 10$^{\text{th}}$ of April, which can be seen in both the CrIS and IASI retrievals. The cloud dissipates by the 15$^{\text{th}}$ of April in the CrIS retrieval reaching just above or near noise levels for both instruments (see Figure A1 in Appendix A for more scenes), which is as expected as the volcano was still venting ash but less vig-

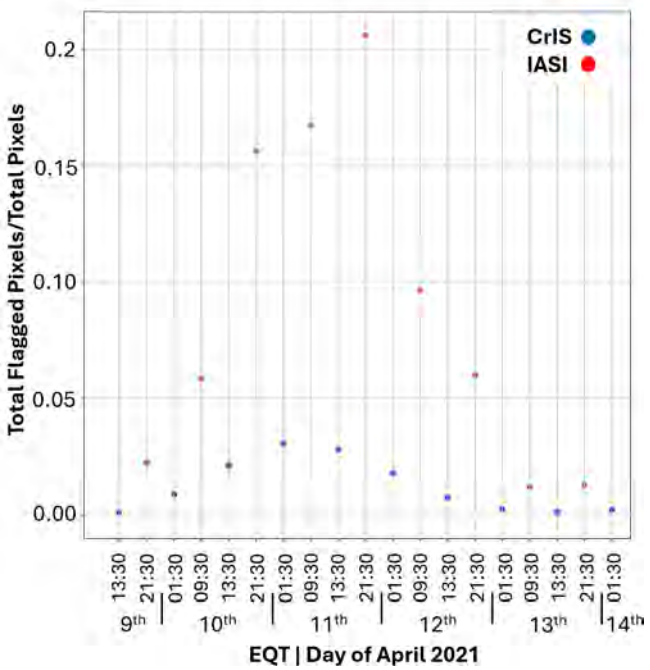

Figure 4: Total flagged pixels over total pixels for the April 2021 eruption of La Soufrière for CrIS and IASI linear retrievals. All times are local times.

orously than before [20].

Figure 4 shows the fraction of flagged pixels over total pixels against time for the CrIS and IASI retrievals. This shows both retrievals agree well on the duration and time profile of the volcanic cloud. However, there are differences: the retrieval run with IASI flags a much greater proportion of pixels when the cloud is visible, and indeed flags around 6.5 times more pixels over the target area between the 10^{th} and 12^{th} of April. The greater sensitivity observed in the IASI retrievals are likely due to two main factors: first, IASI has a finer spectral resolution of 0.25 cm^{-1}, compared to 0.625 cm^{-1} for CrIS within the relevant wavenumber range. Second, the IASI retrieval uses a broader wavenumber range (680 – 1410 cm^{-1}), whereas the CrIS retrieval uses 650 – 1095 cm^{-1}. Both these factors mean the IASI retrieval contains more spectral information per pixel and help to explain it's increased sensitivity. The instruments also have different temperature resolutions as shown in Table 1. IASI has a better temperature resolution than CrIS for most of the used spectral range of 0.2 – 0.3 K compared with 0.24 – 0.39 K. These factors help explain why the IASI retrieval seems to perform better—with less noise and higher detection rates—than the CrIS retrieval. These factors must be of greater effect to the sensitivity of the retrieval than the increased spatial resolution of CrIS compared with IASI (9 vs 4 pixels per 48 x 48 km cell).

Table 3: Summary stats for different covariance matrices

Covariance Matrix	Total Pixels in April 2021	Region Size (million km²)	Percentage Land Cover (%)
Small	347,370	1.60	0
Medium	1,716,506	9.58	0.99
Large	8,160,054	39.9	18.2

Figure 5 compares some of the Washington VAAC ash advisories alongside this paper's CrIS ash retrievals. When ash is reported in the Washington VAAC jurisdiction, an analyst will immediately begin gathering information about the volcanic event [21]. The analyst prepares a volcanic ash advisory including the current vertical and horizontal extent of the ash cloud if it is detectable in satellite imagery. A senior meteorologist at the VAAC will then run a dispersion model for the +6, +12, and +18 hour forecasted ash cloud [21]. The analyst will confirm this forecast with satellite imagery and any other observed data and if satisfied will distribute the advisory. The ash advisories are updated at least every 6 hours, or more if the cloud changes significantly [21]. Figure 5 only uses the contemporaneous ash guidance for each scene. There appears to be good agreement between the official aviation guidance and the CrIS retrievals demonstrating the potential of the CrIS linear ash retrieval for identifying ash clouds.

3.1.1 Changing Covariance Matrices

As explained in Section 2, the mean spectra and covariance matrices are formed from a climatological sample one year before the eruption. In the case of La Soufrière, data for the whole of April 2021 was collected. To explore the impact of the size of the climatological sample region on the retrieval, mean spectra and covariance matrices were generated using 'small', 'medium', and 'large' sized regions around La Soufrière (the red boxes in Figure 6) and separate retrievals were run with the resulting data. Some statistics for the covariance matrices are given in Table 3.

The large region contains a significant amount of land and higher latitudes so contains lots of unrepresentative data for the region the volcanic cloud was tracked through. The small region contains twenty times fewer data points but has 0% land cover and is a much more representative sample for the retrieval region. The medium region is a compromise between the two. Figure 7 shows a selection of scenes for the La Soufrière CrIS retrievals using the small, medium, and

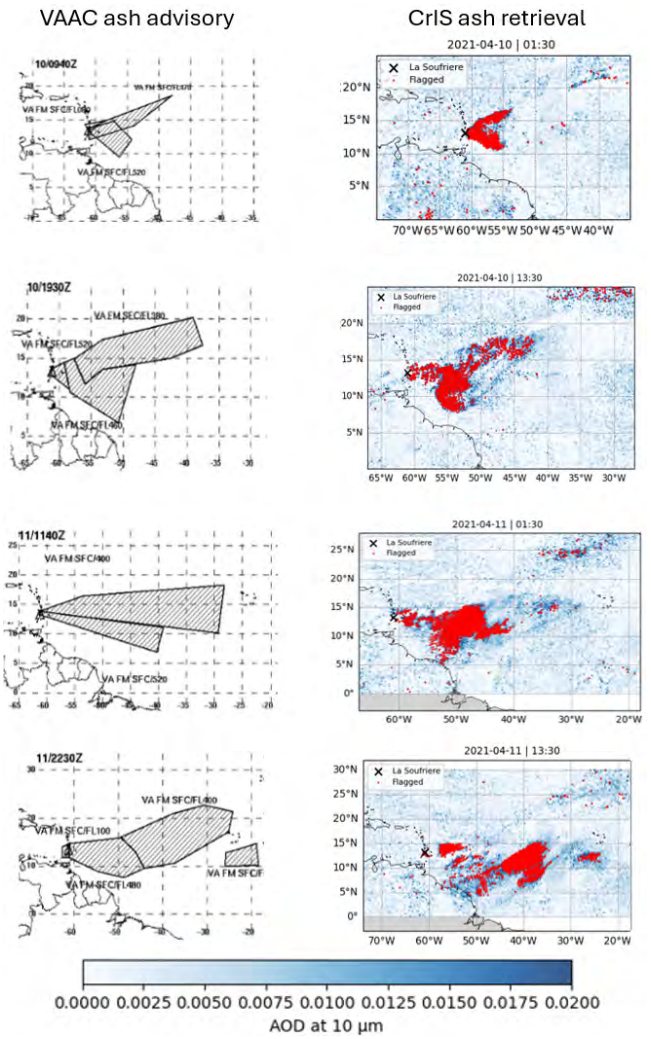

Figure 5: Washington VAAC [7] ash advisory (left) compared with nearest in time CrIS ash retrieval (right).

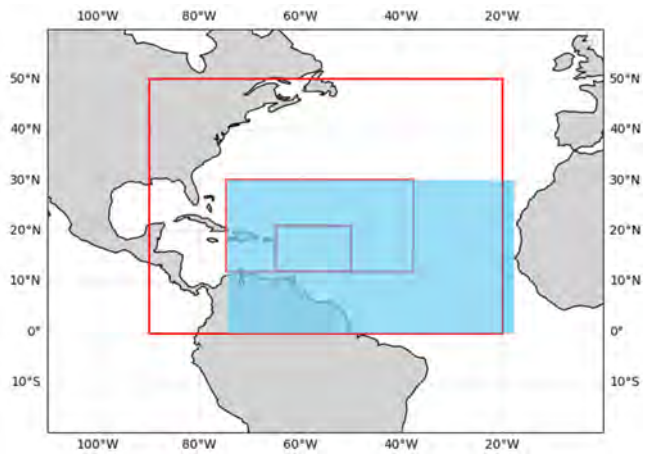

Figure 6: Large, medium, and small regions used to generate covariance matrices (red boxes) and region processed by the CrIS retrieval (blue shaded box).

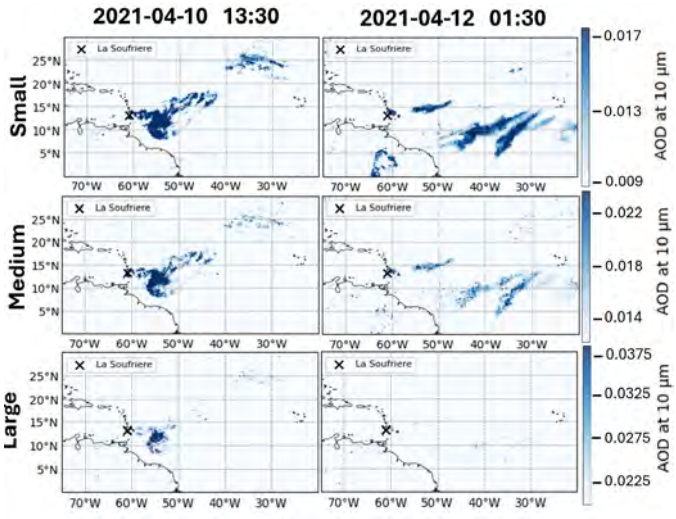

Figure 7: Selection of CrIS ash retrievals for the April 2021 La Soufrière eruption using covariance matrices generated with different sized sample regions.

large sample regions. The colour bar on this figure has an AOD range of 6 to 12 standard deviations above zero in order to allow a fairer comparison—the retrieved AODs will have different distributions between retrievals but the method is qualitative and so only the perceived shape of the ash cloud is of interest. Figure 7 shows both the small and medium retrieval clearly pick out the volcanic cloud, while the large region has lower contrast and so only picks out part of the ash cloud. This demonstrates the need for the retrieval to use representative sample regions. The small retrieval shows noise over land for the observation on the 12$^{\text{th}}$ at 01:30 LT, whereas the medium and large retrievals show much less noise over land, indicating that the increased size of these regions may make the retrievals more robust to different types of climatology. This suggests that using a large climatological region could be advantageous if using the retrieval over a larger and more varied area.

3.1.2 Changing Jacobians

As discussed in Section 2.1 the Jacobian is the measure of how much the brightness temperature spectra should change when adding a layer of ash with an AOD of one to the atmosphere. Retrievals shown so far used a Jacobian generated by feeding a 2 km thick layer of ash at a 20 km altitude into the RFM. The effect of the modelled ash height fed into the RFM on the retrieval was investigated by generating three different Jacobians by inputting ash at three different heights (10, 15, and 20 km) into the RFM.

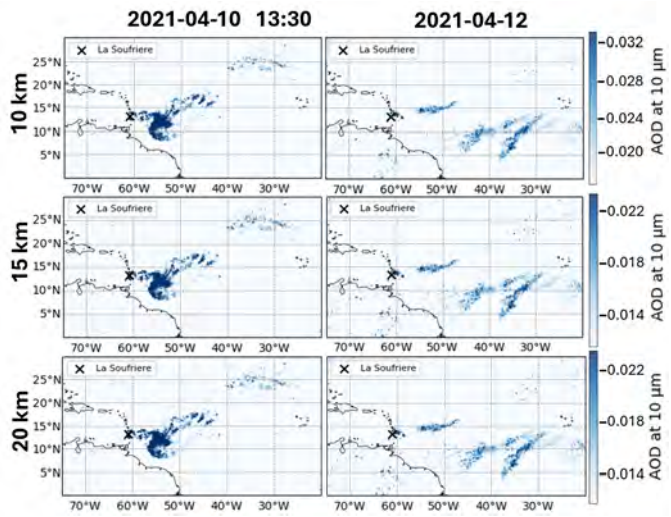

Figure 8: Selection of CrIS ash retrievals for the April 2021 La Soufrière eruption using Jacobians generated with different modelled ash layer heights.

Figure 8 shows selected scenes for the CrIS ash retrievals of the April 2021 La Soufrière eruption generated using these different Jacobians. As in Figure 7 the colour bars on this figure have an AOD range of 6 to 12 standard deviations above zero. The figure shows no noticeable difference between the retrievals indicating that the modelled height of the ash cloud has little effect on the retrieval, at least for this eruption.

3.2 Hunga Tonga-Hunga Ha'apai

HT-HH is a submarine volcano in the South Pacific, in the Kingdom of Tonga [20]. It has erupted several times since the first (recorded) eruption in 1912 [20]. This paper looks at the eruptions beginning on the 14$^{\text{th}}$ of January 2022. This includes a very large eruption on the 15$^{\text{th}}$ of January which generated a plume that reached 57 km [22], the highest ever recorded. The umbrella cloud expanded to a diameter of 600 km in under 2.5 hours [20]. This eruption increased the mass of water vapour in the stratosphere by $\sim$ 10% [23] and as a result it is disputed whether this caused net cooling (through increased atmospheric aerosols) as is more typical for stratospheric eruptions or net warming through an increase in radiative forcing from this excess water vapour [23].

The CrIS ash retrieval output for the HT-HH eruption is shown in Figure 9. The cloud is tracked from the initial eruption on the 14$^{\text{th}}$ of January until 17$^{\text{th}}$. Figure 9 agrees well with the chronology of the eruption before the ash cloud reaches Australia. A few pixels are flagged on the 14$^{\text{th}}$ at 13:30 LT and a few more on the next observation at 01:30 LT on the 15$^{\text{th}}$. Ash is then not detected on the 15$^{\text{th}}$ at 13:30 LT. This agrees well with the eruption timeline; GVP [20] reports an eruption beginning at 04:20 LT on the 14$^{\text{th}}$ of January, expanding rapidly to around 250 km ($\sim$ 2.5 degrees) and ending around 12 hours later.

GVP [20] then reports intermittent activity until a larger eruption at 17:00 LT on the 15$^{\text{th}}$ with, as mentioned, the volcanic cloud diameter growing to at least 600 km ($\sim$ 5.5 degrees) by 19:03 LT. The ash flags of the CrIS retrieval on the 16$^{\text{th}}$ at 01:30 LT span around 3 or 4 degrees so this is a reasonable agreement. This paper's ash retrieval then shows the ash cloud expanding significantly and travelling west, reaching Australia on the 17$^{\text{th}}$ at around 13:30 LT. This was the limit of the processed data available. Tracking the ash cloud over Australia using this method would have been very difficult due to the large number of false detections over the continent. This can be seen in the 13:30 LT observation on the 16$^{\text{th}}$ in Figure 9, which shows many flags over Australia before the cloud had reached the continent, showing that the linear retrieval struggles to distinguish between dust and ash. This likely results from desert land surfaces and desert dust being spectrally similar to volcanic ash [14]. Generating separate mean spectra and covariance matrices over Australia might help to alleviate this issue. There are far fewer false detections for night time observations. Improved thermal contrast between the volcanic cloud and the surface—with surface temperatures significantly cooler at night than during the day in the Australian summer—likely explains this.

Figure 10 shows some selected scenes for the CrIS retrieval alongside some selected scenes from Figure 1 of Sellitto et al [18]. Sellitto uses a composite brightness temperature difference method to create an RGB colour map. The method takes differences between spectral channels with known sensitivity to volcanic gases and aerosols as parameters for the strength of each colour. This results in thick ice or ash clouds appearing brown, thin ice clouds appearing dark blue and clouds containing sulphur appearing green. Figure 10 shows a good collocation between the sulphur clouds of Sellitto's scenes (green) and the ash clouds of the CrIS retrieval on the 16$^{\text{th}}$ and 17$^{\text{th}}$ (17$^{\text{th}}$ shown in Figure A2 in Appendix A). This matches predictions as volcanic sulphur and ash clouds are often co-

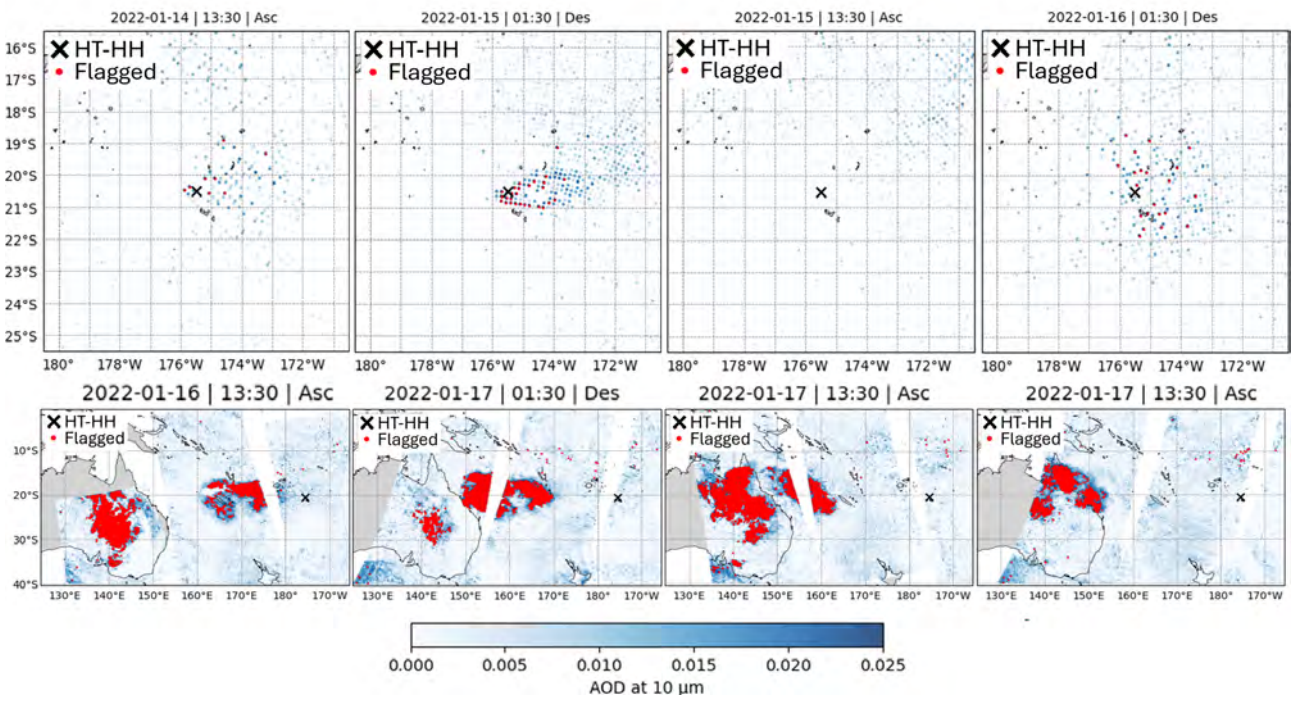

Figure 9: CrIS ash retrieval for the January 2022 eruption of HT-HH. Times are local.

located [24]. The optically thick ice/ash cloud visible over HT-HH on the 15th at 22:00 LT for the RGB scene is much larger than the cloud detected in the CrIS retrieval on the 16th at 01:30 LT. This could be due to the cloud containing a significant amount of ice which the CrIS retrieval would not flag as ash.

4 Conclusions

In this study, the Walker et al [1] linear retrieval method has been adapted to detect ash with the CrIS instrument. The study has demonstrated that this produces convincing volcanic ash cloud distributions that agree well with similar methods developed for IASI and with professional ash guidance produced by the Washington VAAC. This demonstrates the method's potential to be used to improve volcanic ash guidance globally and to double the temporal resolution of the ash tracking done in EODG. However, the method has limitations, summarised in Table 2. Further work should aim to: demonstrate and validate the approach across a wider range of eruptions; develop a smarter thresholding technique to decrease false positives; conduct thorough validation using satellite data, radiosondes, and ground-based observations; and devise a calibration strategy to convert retrieved AOD values into ash mass concentrations. This calibration is critical, as aviation safety guidelines use mass ash concentration thresholds to determine whether airspace is safe for flight.

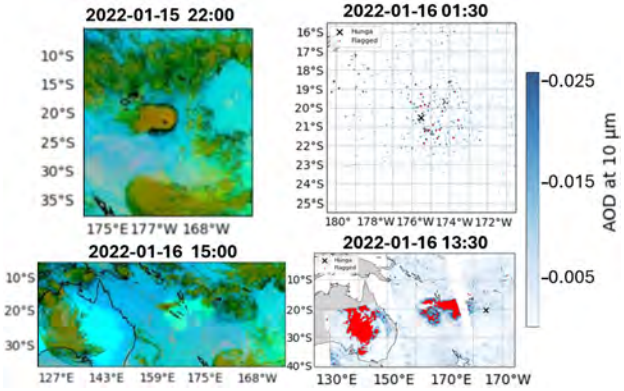

Figure 10: RGB colour map from Sellitto et al [18] (left) and CrIS linear ash retrieval for selected scenes of the January 2022 eruption of HT-HH.

References

[1] J. C. Walker et al. "An effective method for the detection of trace species demonstrated using the MetOp Infrared Atmospheric Sounding Interferometer". In: *Atmospheric Measurement Techniques* 4.8 (2011), pp. 1567–1580.

[2] National Weather Service. *Volcanic Ash and Ashfall.* last access: 29 November 2024. URL: `https://www.weather.gov/safety/airquality-volcanic-ash`.

[3] J. A. Stevenson. *A history of ash clouds and aviation*. last access: 29 November 2024. URL: https://all-geo.org/volcan01010/2014/02/a-history-of-ash-clouds-and-aviation/.

[4] J. A. Stevenson. *Grímsvötn 2011 (Part 2): Effects on aviation of the biggest Icelandic eruption since Katla 1918*. last access: 29 November 2024. URL: https://all-geo.org/volcan01010/2013/07/grimsvotn-2011-in-uk-part-2-aviation/.

[5] R. Sparks et al. "Monitoring Volcanoes". In: *Science (New York, N.Y.)* 335.1310 (2012), pp. 1310–1.

[6] M. J. Pavolonis et al. "Automated Detection of Explosive Volcanic Eruptions Using Satellite-Derived Cloud Vertical Growth Rates". In: *Earth and Space Science* 5.12 (2018), pp. 903–928.

[7] NOAA. *Washington VAAC volcanic ash advisory notices*. last access: 21 March 2025. URL: https://www.ospo.noaa.gov/products/atmosphere/vaac/.

[8] World Meteorological Organization. *Observing Systems Capability Analysis and Review Tool*. last access: 19 February 2024. URL: https://space.oscar.wmo.int/instruments.

[9] A. J. Prata. "Observations of volcanic ash clouds in the 10–12 μm window using AVHRR/2 data". In: *International Journal of Remote Sensing* 10.4–5 (1989), pp. 751–761.

[10] C. D. Rodgers. *Inverse Methods for Atmospheric Sounding: Theory and Practice*. World Scientific, 2000.

[11] A. Dudhia. *Reference Forward Model web page*. last access: 12 February 2025. URL: https://eodg.atm.ox.ac.uk/RFM/.

[12] A. Smith. *Thoughts about covariance*. last access: 19 February 2024. 2013. URL: https://eodg.atm.ox.ac.uk/eodg/gray/2013Smith.pdf.

[13] R. Tichford. *Can we improve our detection of volcanic clouds by creating more representative covariance matrices?* last access: 19 February 2025. 2024. URL: https://eodg.atm.ox.ac.uk/eodg/vacation_reports/2024Tichford.pdf.

[14] I. A. Taylor et al. "Investigating the use of the Saharan dust index as a tool for the detection of volcanic ash in SEVIRI imagery". In: *Journal of Volcanology and Geothermal Research* 304 (2015), pp. 126–141.

[15] B. Pery. *Detecting sulphur dioxide emissions from volcanoes with the Cross-track Infrared Sounder*. last access: 29 November 2024. 2023. URL: https://eodg.atm.ox.ac.uk/eodg/mphys_reports/2023_Pery.pdf.

[16] F. Iturbide-Sanchez and CrIS SDR Team. *NOAA-20 CrIS SDR Validated Maturity Review*. last accessed: 25 April 2025. 2018. URL: https://www.star.nesdis.noaa.gov/jpss/documents/AMM/N20/CrIS_SDR_Validated.pdf.

[17] I. A. Taylor et al. "A satellite chronology of plumes from the April 2021 eruption of La Soufrière, St Vincent". In: *Atmospheric Chemistry and Physics* 23.24 (2023), pp. 15209–15234.

[18] P. Sellitto et al. "The unexpected radiative impact of the Hunga Tonga eruption of 15th January 2022". In: *Communications Earth & Environment* 3 (2022), p. 288.

[19] R. E. A. Robertson et al. "The 2020–21 Eruption of La Soufrière Volcano, St Vincent". In: *Geological Society, London, Special Publications* 539 (2024), pp. 1–24.

[20] Smithsonian Institution, National Museum of Natural History, Global Volcanism Program. *Global Volcanism Program*. last access: 18 February 2024. URL: https://volcano.si.edu/.

[21] National Weather Service. *Volcanic Ash Advisory Centers: Operations and Responsibilities*. last accessed: 25 April 2025. 2018. URL: https://www.weather.gov/media/directives/010_pdfs_archived/pd01015001b.pdf.

[22] S. R. Proud et al. "The January 2022 eruption of Hunga Tonga-Hunga Ha'apai volcano reached the mesosphere". In: *Science (New York, N.Y.)* 378.6619 (2022), pp. 554–557.

[23] L. Millán et al. "The Hunga Tonga-Hunga Ha'apai Hydration of the Stratosphere". In: *Geophysical Research Letters* 49.13 (2022), e2022GL099381.

[24] D. M. Hyman et al. "Probabilistic retrieval of volcanic SO_2 layer height and partial column density using the Cross-track Infrared Sounder (CrIS)". In: *Atmospheric Measurement Techniques* 13.11 (2020), pp. 5891–5921.

A Additional Figures

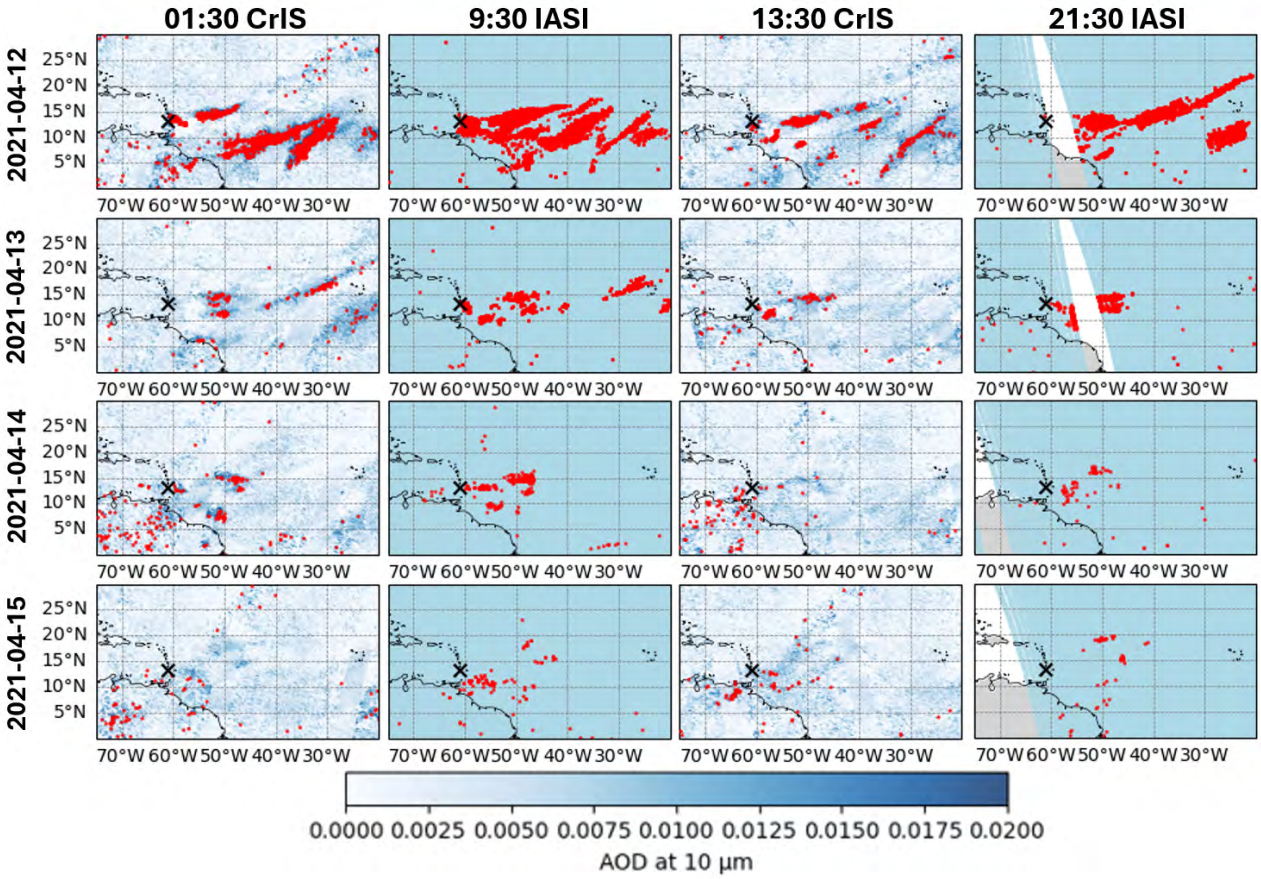

Figure A1: Further scenes of the CrIS and IASI retrievals for the April 2021 eruption of La Soufrière. All times local.

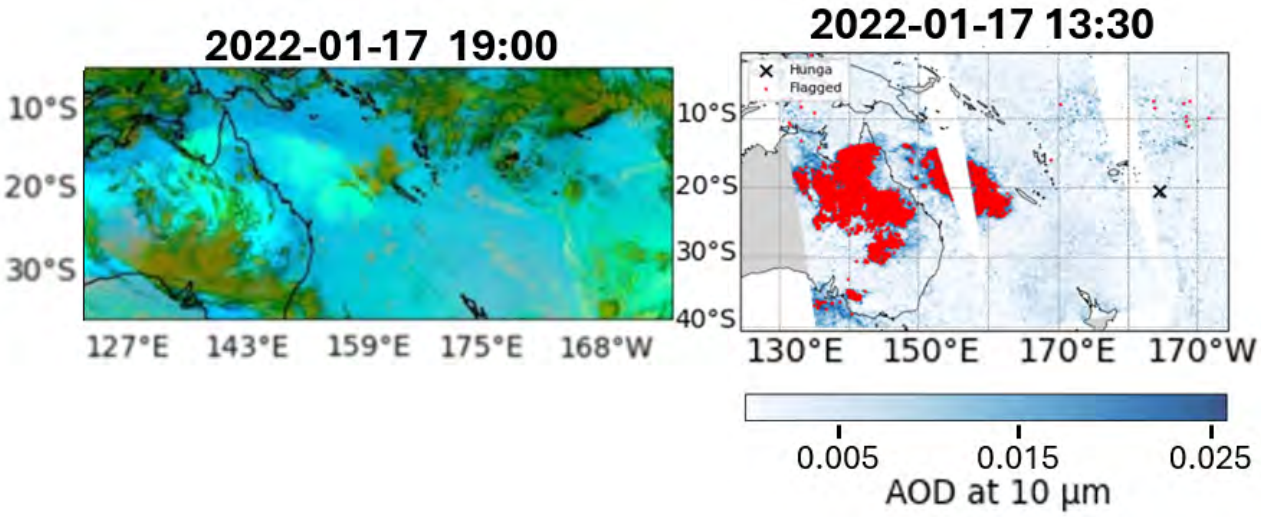

Figure A2: RGB colour map from Sellitto et al [18] (left) and CrIS linear ash retrieval for 17th of January 2022 scene for eruption of HT-HH.